Chemical Science

ROYAL SOCIETY OF CHEMISTRY

EDGE ARTICLE

View Article Online
View Journal | View Issue

Check for updates

Cite this: *Chem. Sci.*, 2024, **15**, 15440

All publication charges for this article have been paid for by the Royal Society of Chemistry

Received 16th July 2024
Accepted 24th August 2024

DOI: 10.1039/d4sc04711g

rsc.li/chemical-science

Oxygen-bridged W-Pd atomic pairs enable H_2O_2 activation for sensitive immunoassays†

Chengjie Chen,[a] Dongbo Yan,[a] Xiangkun Jia,[a] Ruimin Li,[a] Lijun Hu,[a] Xiaotong Li,[a] Lei Jiao, *[a] Chengzhou Zhu, [b] Yanling Zhai*[a] and Xiaoquan Lu [a]

Regulating the performance of peroxidase (POD)-like nanozymes is a prerequisite for achieving highly sensitive and accurate immunoassays. Inspired by natural enzyme catalysis, we design a highly active and selective nanozyme by loading atomically dispersed tungsten (W) sites on Pd metallene (W-O-Pdene) to construct an artificial three-dimensional (3D) catalytic center. The 3D asymmetric W-O-Pd atomic pairs can effectively stretch the O–O bonds in H_2O_2 and further promote the desorption of H_2O to enhance POD-like activity. Moreover, the W-O-Pd sites with unique spatial structures demonstrate satisfactory specificity for H_2O_2 activation, effectively preventing the interference of dissolved oxygen. Accordingly, the highly active and specific W-O-Pdene nanozymes are utilized for sensitive and accurate prostate-specific antigen (PSA) immunoassay with a low detection limit of 1.92 pg mL^{-1}, superior to commercial enzyme-linked immunosorbent assay.

Open Access Article. Published on 26 August 2024. Downloaded on 2/8/2026 1:38:20 PM.
This article is licensed under a Creative Commons Attribution-NonCommercial 3.0 Unported Licence.

Introduction

Nanozymes with POD-like activity have become effective substitutes for natural POD and have been extensively investigated for colorimetric immunoassay.[1–6] Understanding and regulating the H_2O_2 activation of POD-like nanozymes plays a key role in improving the sensitivity and accuracy of immunoassay.[7–10] Although POD-like nanozymes have witnessed enormous progress in enhancing catalytic activity, limited studies have demonstrated improvement in catalytic specificity.[11,12] Although several efforts have been devoted to addressing this issue,[13–15] the rational design and controllable preparation of specific POD-like nanozymes are still impeded by an incomplete understanding of the reaction mechanism.[16,17] In particular, due to the structural complexity of nanozymes, the selective cleavage of the O–O bond in H_2O_2 activation is still ambiguous.[18–21]

Horseradish peroxidases (HRP) are state-of-the-art biocatalysts and their catalytic pockets with unique electronic and geometrical structures significantly facilitate H_2O_2 activation.[22,23] In their three-dimensional catalytic pockets, the synergistic effects between catalytic sites and binding sites can accelerate the proton-coupled electron transfer of selective H_2O_2 activation.[24–26] The strong affinity between the H_2O_2 molecule and enzyme gives HRP excellent catalytic selectivity.[27] Hence, to significantly improve the catalytic activity and selectivity of nanozymes for H_2O_2 activation, rational design of the active sites of nanozymes requires vivid mimicking of the catalytic pocket of HRP. Not only the binding and catalysis sites but also the spatial configuration of the active sites should be designed.

Herein, W-O-Pdene nanozymes with artificial 3D catalytic centers (asymmetric W-O-Pd sites) are synthesized successfully as highly efficient POD mimics. Asymmetric W-O-Pd sites can provide the catalytic and binding sites for H_2O_2 activation, which not only improve the H_2O_2 adsorption but also reduce the energy barrier of H_2O desorption, thus efficiently achieving the improvement of H_2O_2 activation efficiency. Besides, owing to the unique spatial configuration, W-O-Pd sites can stretch the O–O bond of H_2O_2 and compress the O–O bond of O_2, resulting in selectively enhanced POD-like activity, effectively preventing the interference of dissolved oxygen. Accordingly, W-O-Pdene nanozymes display more than 6 times higher POD-like activity and better affinity for H_2O_2 than pure Pd metallene (Pdene) nanozymes. Finally, W-O-Pdene nanozymes are used in the immunoassay of the PSA, demonstrating an ultra-low limit (1.92 pg mL^{-1}) and practical feasibility in clinical diagnosis.

Results and discussion

Fig. 1a exhibits a schematic diagram of the fabrication procedure of Pdene and W-O-Pdene nanozymes. The homogeneous reaction mixture, consisting of $W(CO)_6$, ascorbic acid, and $Pd(acac)_2$, was heated at 80 °C for one hour to obtain Pdene. In

[a]*Institute of Molecular Metrology, College of Chemistry and Chemical Engineering, Qingdao University, Qingdao 266071, P. R. China. E-mail: zhaiyanling@qdu.edu.cn; jiaolei@qdu.edu.cn*

[b]*National Key Laboratory of Green Pesticide, International Joint Research Center for Intelligent Biosensing Technology and Health, College of Chemistry, Central China Normal University, Wuhan 430079, P. R. China*

† Electronic supplementary information (ESI) available. See DOI: https://doi.org/10.1039/d4sc04711g

© 2024 The Author(s). Published by the Royal Society of Chemistry

Open Access Article. Published on 26 August 2024. Downloaded on 2/8/2026 1:38:20 PM. This article is licensed under a Creative Commons Attribution-NonCommercial 3.0 Unported Licence.

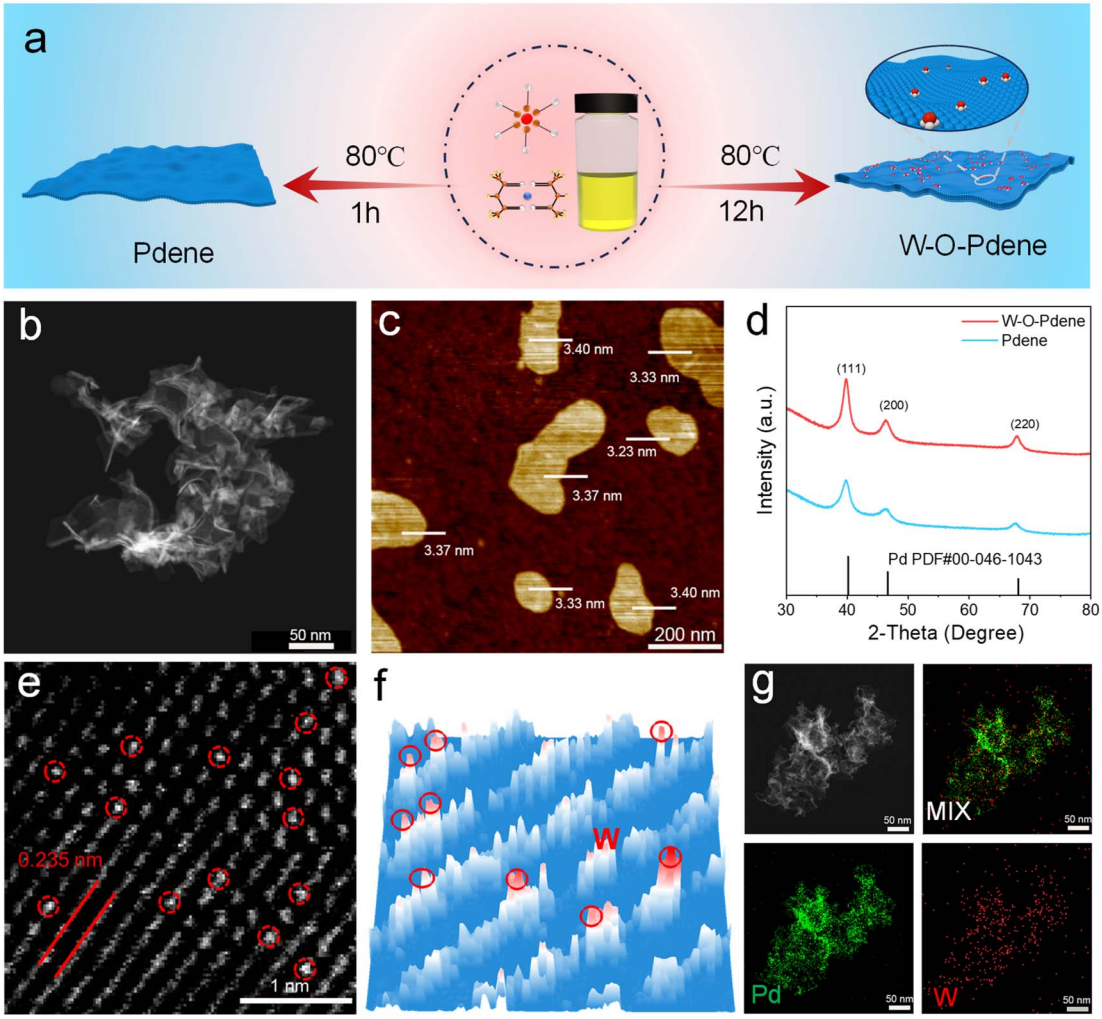

Fig. 1 (a) Scheme of the preparation of Pdene and W-O-Pdene. (b) HAADF-STEM image of W-O-Pdene. (c) AFM image of W-O-Pdene. (d) XRD spectra of W-O-Pdene and Pdene. (e) AC-HAADF-STEM image of W-O-Pdene. (f) 3d intensity profile of W-O-Pdene. (g) Elemental mapping of W-O-Pdene.

the process, the temperature-induced decomposition of $W(CO)_6$ led to the emission of carbon monoxide (CO), which acted as a ligand directing the atomic arrangement. The CO ligand exhibits a preference for binding to the low-index (111) facet of Pd, thereby facilitating anisotropic growth. W-O-Pdene with oxygen-bridged W-Pd atomic pairs is obtained after heating for 12 h. Transmission electron microscopy (TEM) and high-angle annular dark-field scanning TEM (HAADF-STEM) images provide evidence that the Pdene and W-O-Pdene exhibit a crosslinked curved 2D nanostructure (Fig. 1b and S1a, b,†). Moreover, the atomic force microscopy (AFM) images of Pdene and W-O-Pdene indicate an average thickness of only 1.2 nm and 3.4 nm, respectively (Fig. 1c and S2†). As described, W-O-Pdene possesses ultra-thin characteristics that can provide more active sites. The X-ray diffraction (XRD) pattern of W-O-Pdene indicates good crystallinity, which is consistent with the selected area electron diffraction (SAED) result (Fig. 1d and S3†). The diffraction peaks at 39.6, 45.8, and 67.3 are indexed to the 111, 200, and 220 planes of the fcc structure of W-O-Pdene. Aberration-corrected HAADF-STEM (AC-HAADF-STEM) characterization was performed. As illustrated in Fig. 1e and f, the heavy element W appears as dense bright contrast dots within the red circles. W-O-Pdene exhibits a lattice spacing of 0.235 nm, consistent with the high-resolution TEM images of Pdene and W-O-Pdene (Fig. S4†). Besides, the energy-dispersive X-ray spectroscopy elemental mapping demonstrates the homogenous distribution of Pd and W elements within the W-O-Pdene (Fig. 1g).

The chemical state of W-O-Pdene and Pdene was investigated by X-ray photoelectron spectroscopy (XPS). The location of the Pd^0 peaks of W-O-Pdene in the Pd 3d spectra at 335.7 eV and 341.0 eV suggests a negative shift in comparison to Pdene (335.9 eV and 341.2 eV), indicating a clear electronic interaction (Fig. 2a). As displayed in Fig. 2b, two weak peaks at 37.7 eV and 35.5 eV can be attributed to W $4f_{5/2}$ and W $4f_{7/2}$ in W-O-Pdene. Notably, most of the W exists in the W^{6+} state, and no discernible peaks attributed to W^0 are observed. X-ray absorption near-edge structure (XANES) and extended X-ray absorption fine structure (EXAFS) analyses were utilized to investigate the electronic structure and coordination environment in W-O-

Open Access Article. Published on 26 August 2024. Downloaded on 2/8/2026 1:38:20 PM.
This article is licensed under a Creative Commons Attribution-NonCommercial 3.0 Unported Licence.

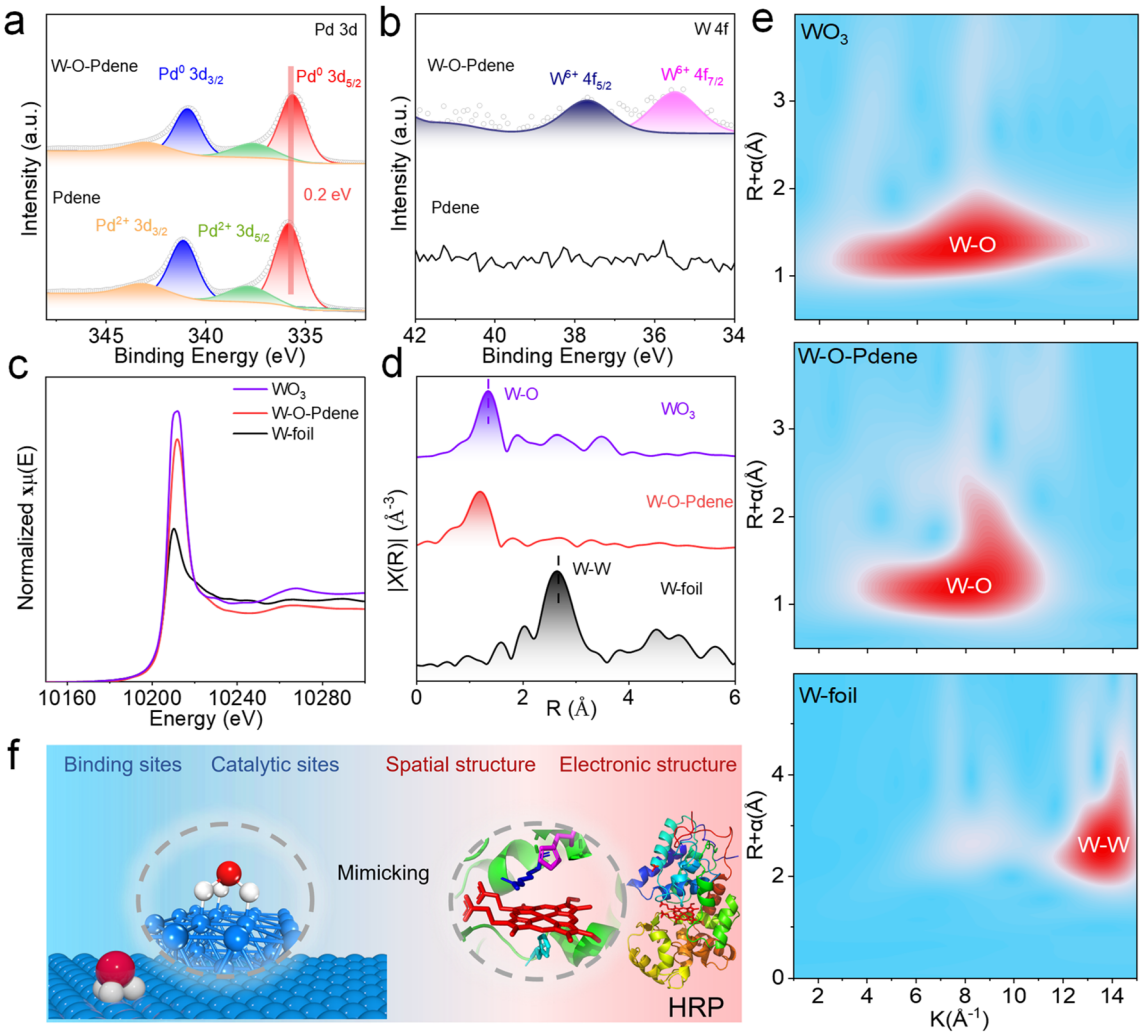

Fig. 2 XPS spectra of W-O-Pdene and Pdene for Pd 3d (a) and W 4f (b). (c) W L-edge XANES spectra of WO_3, W-O-Pdene, and W foil. (d) FT-EXAFS spectra of WO_3, W-O-Pdene, and W foil. (e) WT images of WO_3, W-O-Pdene, and W-foil. (f) W-O-Pdene and the HRP structural model diagram.

Pdene. The white line intensity of W-O-Pdene is between that of W-foil and WO_3, indicating that the valence state of W is between 0 and 6 (Fig. 2c). Meanwhile, the Fourier transform W L-edge EXAFS (FT-EXAFS) spectra of W-O-Pdene reveal a single peak centered at 1.2 Å, corresponding to the W–O scattering path (Fig. 2d). In particular, the absence of the W–W peak in the FT-EXAFS spectra confirms the atomic distribution of W. Fig. S5† presents the EXAFS fitting curves, and Table S1† provides the fitting results of W-O-Pdene. The coordination number of the W–O shell is about 3. Furthermore, wavelet transform (WT) analysis was employed (Fig. 2e). The maximum intensity of the W-foil is about 13.6 $Å^{-1}$, which corresponds to the W–W bond. The maximum intensity of W-O-Pdene is about 8.1 $Å^{-1}$, which is like that of WO_3 and corresponds to the W–O bond. Based on these results, the geometric configuration is optimized through first-principles calculations (Fig. S6†). In the most stable configuration of W-O-Pdene, W atoms are anchored on Pdene with three oxygen bridges. As displayed in Fig. 2f, the W-O-Pdene nanozyme possesses a spatially stable 3D structure. W-O-Pd asymmetric sites are successfully constructed as artificial 3D catalytic centers, and the W atom provides binding sites and catalytic sites for H_2O_2 activation. Like the HRP catalytic pocket, the artificial 3D catalytic centers possess unique spatial and electronic structures and can potentially enhance nanozyme activity and specificity.[28–31]

The typically chromogenic reaction (TMB/H_2O_2) was used to verify the POD-like activity of W-O-Pdene and Pdene. As displayed in Fig. 3a, the W-O-Pdene can rapidly oxidize TMB and produce an obvious absorbance change at 652 nm with the assistance of H_2O_2, and the absorbance of the W-O-Pdene system is higher than that of the Pdene system. Without nanozymes, the TMB/H_2O_2 system cannot trigger the absorbance changes. As shown in Fig. S7,† the Michaelis–Menten equation verified the kinetic analysis of the POD-like activity of different nanozymes at different concentrations of H_2O_2 and TMB, respectively. Table S2† displays the kinetic constants (V_{max} and K_m). On the one hand, W-O-Pdene nanozymes possess higher V_{max} for both H_2O_2 and TMB than Pdene nanozymes, showing their higher catalytic activity; on the other hand, W-O-Pdene nanozymes have lower K_m value than Pdene, which

© 2024 The Author(s). Published by the Royal Society of Chemistry

Open Access Article. Published on 26 August 2024. Downloaded on 2/8/2026 1:38:20 PM.
This article is licensed under a Creative Commons Attribution-NonCommercial 3.0 Unported Licence.

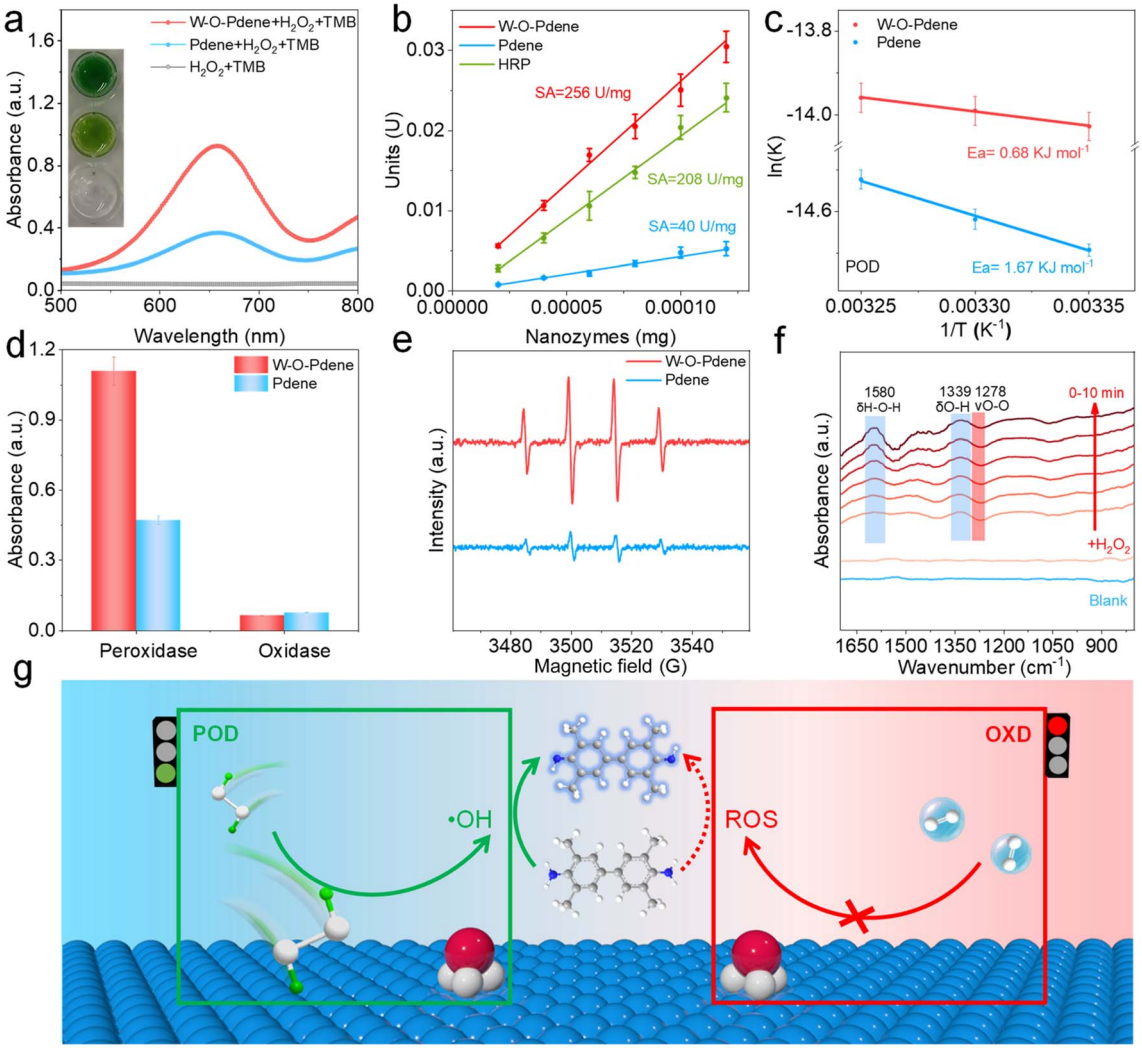

Fig. 3 (a) Absorbance spectra of the H_2O_2-TMB system catalyzed by W-O-Pdene and Pdene. (b) The specific activity of W-O-Pdene, Pdene, and HRP. (c) E_a of W-O-Pdene and Pdene in H_2O_2 activation. (d) POD-like and OXD-like activity of W-O-Pdene and Pdene. (e) EPR spectra of W-O-Pdene and Pdene. (f) *In situ* ATR-FTIR spectra of the H_2O_2 catalytic reaction on W-O-Pdene. (g) Schematic of W-O-Pdene for H_2O_2 and O_2 activation.

indicates that W-O-Pdene has a better affinity to H_2O_2. The specific activity (SA) is defined as activity units per milligram of nanozymes which can quantitatively evaluate the POD-like activity.[32] As shown in Fig. 3b, the SA of W-O-Pdene (256 U mg^{-1}) increases more than 6 times compared with Pdene (40 U mg^{-1}) and is higher than that of HRP (208 U mg^{-1}), which means that W-O-Pdene has better H_2O_2 catalytic activity than Pdene and HRP. As shown in Table S3,† compared to noble metal nanoparticle nanozymes, W-O-Pdene nanozymes have the best POD-like activity. The activation energy (E_a) of POD-like activity was calculated based on the Arrhenius equation to reveal the catalytic mechanism.[33–35] As displayed in Fig. 3c, W-O-Pdene nanozymes (0.68 KJ mol^{-1}) have a lower E_a value for POD-like activity than that of Pdene nanozymes (1.67 KJ mol^{-1}), indicating that W-O-Pdene nanozymes can better express POD-like activity. Like natural HRP, W-O-Pdene nanozymes display pH-dependent characteristics (Fig. S8a†). Compared with natural HRP, W-O-Pdene nanozymes possess high-temperature tolerance (Fig. S8b†). Meanwhile, W-O-Pdene has better recyclability than HRP; after five cycles the POD-like activity remained unchanged (Fig. S8c†). XRD (Fig. S9a†) and TEM (Fig. S9b†) of W-O-Pdene after the reaction have not changed, indicating that W-O-Pdene has excellent stability.

In addition to POD-like activity, nanozymes usually have oxidase (OXD)-like activity which can catalyze O_2 and oxidize chromogenic substrates, seriously affecting the accuracy of immunoassay. Herein, the OXD-like and POD-like activities of W-O-Pdene nanozymes and Pdene nanozymes are investigated (Fig. 3d). Impressively, compared with Pdene, W-O-Pdene nanozymes possess lower OXD-like and higher POD-like activity, demonstrating that W-O-Pdene nanozymes can enhance POD-like activity and decrease OXD-like activity. As shown in Fig. S10,† the Michaelis–Menten equation verifies the kinetic analysis of the OXD-like activity of the W-O-Pdene nanozymes and Pdene nanozymes at different concentrations of TMB. W-O-Pdene nanozymes have lower V_{max} and higher K_m

Open Access Article. Published on 26 August 2024. Downloaded on 2/8/2026 1:38:20 PM. This article is licensed under a Creative Commons Attribution-NonCommercial 3.0 Unported Licence.

than that of Pdene nanozymes, indicating that Pdene nanozymes have better O_2 catalytic activity (Table S4†). Electrochemical tests were performed to further verify the specificity of the nanozymes, using nanozyme-modified glassy carbon electrodes to evaluate the catalytic activity of H_2O_2 and O_2. As displayed in Fig. S11a,† W-O-Pdene nanozymes demonstrate a larger H_2O_2 reduction current than that of Pdene nanozymes, indicating that W-O-Pdene nanozymes have outstanding H_2O_2 reduction activity. In contrast, Fig. S11b† indicates that W-O-Pdene nanozymes have excellent specificity for H_2O_2 activation. These results convincingly demonstrate that W-O-Pdene nanozymes possess excellent specificity for H_2O_2 activation. Next, the active intermediates of the POD-like reaction system were confirmed by using isopropanol (IPA) as the ·OH scavenger. As shown in Fig. S12a,† when IPA is added to the POD-like catalytic system, a significant decrease in the absorbance value emerges, indicating that the produced ·OH is one of the active intermediates. Moreover, terephthalic acid (TA) can be used as a typical fluorescent probe to further detect the resulting ·OH. As shown in Fig. S12b and c,† the Fenton reaction system can react with TA and generate an obvious fluorescence signal, indicating that TA can be used as an ·OH fluorescent probe. Similarly, both Pdene and W-O-Pdene reaction systems can also react with TA to generate significant fluorescence signals, which can determine the existence of ·OH intermediates. To obtain deeper insights into the catalytic process, electron paramagnetic resonance (EPR) tests were conducted. 5,5-dimethyl-1-pyrroline N-oxide (DMPO) is used as the spin trap of ·OH. As displayed in Fig. 3e, the higher EPR signal of the W-O-Pdene catalytic system is observed, indicating that more ·OH is produced than that of the Pdene. To examine the other reactive oxygen species, nitro blue tetrazolium chloride (NBT) and Dimethyl sulfoxide (DMSO) were used to detect $\cdot O_2^-$ and absorbed oxygen (*O) respectively. NBT can react with $\cdot O_2^-$ to produce blue absorption at about 560 nm. Fig. S13a† indicates that there is no $\cdot O_2^-$ in the catalytic system. DMSO can scavenge *O and ·OH, and tert-butanol (TBA) can only scavenge ·OH. As displayed in Fig. S13b,† ·OH is the main reactive intermediate in the Pdene nanozyme and W-O-Pdene nanozyme catalytic systems. Then, *in situ* ATR-FTIR spectroscopy was employed to monitor the process of H_2O_2 activation. After the addition of H_2O_2, two signals at 1580 cm^{-1} and 1339 cm^{-1} can be detected respectively (Fig. 3f), which can be assigned to the H–O–H bending mode and O–H of absorbed H_2O_2.[36,37] Besides, peaks at 1278 cm^{-1} can be assigned to the stretching vibration of O–O in H_2O_2, which gradually decreased because of the partial dissociation of H_2O_2.[38] These results indicate that the O–O bond in H_2O_2 can be stretched in the catalytic process (Fig. 3g).

To reveal the internal mechanism of artificial 3D catalytic centers to enhance the activity and specificity of nanozymes, density functional theory (DFT) calculations were performed. At first, the impacts of active sites are evaluated by calculating the

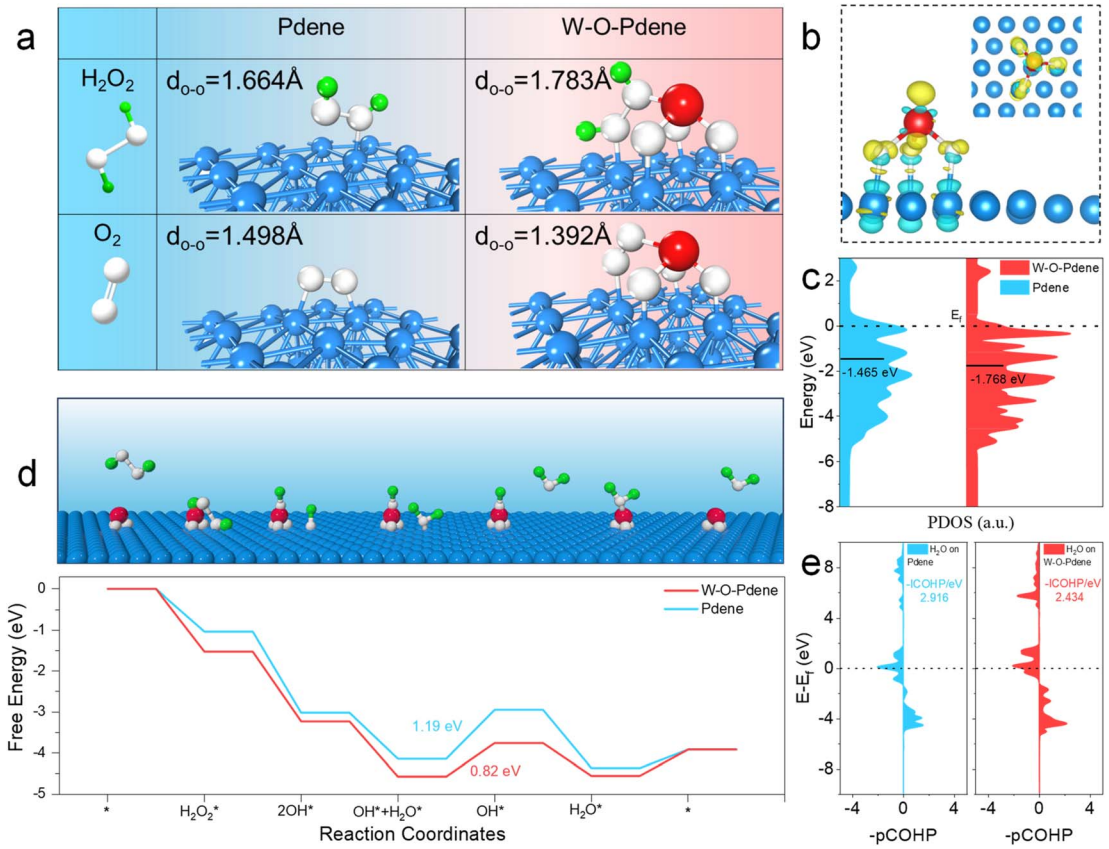

Fig. 4 (a) Distance of O–O in H_2O_2 and O_2 on Pdene and W-O-Pdene, respectively. (b) The charge density difference of W-O-Pdene (yellow: charge accumulation; cyan: charge depletion). (c) PDOS of the Pd d-band for W-O-Pdene and Pdene. (d) Schematic representation of the fundamental reaction step. Energy change diagram of H_2O_2 activation on W-O-Pdene and Pdene. (e) COHP of H_2O* on Pdene and W-O-Pdene.

© 2024 The Author(s). Published by the Royal Society of Chemistry

Open Access Article. Published on 26 August 2024. Downloaded on 2/8/2026 1:38:20 PM. This article is licensed under a Creative Commons Attribution-NonCommercial 3.0 Unported Licence.

O–O bond distance of H_2O_2 and O_2 adsorbed on Pdene and W-O-Pdene (Fig. 4a). The dual active sites (W-O-Pd) of W-O-Pdene nanozymes can alter the adsorption conformation of H_2O_2 and thus achieve the extension of the O–O bond, which facilitates the activation of H_2O_2. Impressively, when O_2 is adsorbed on the W-O-Pd site, the O–O bond of O_2 is compressed and thus inhibits the O_2 activation. Moreover, the analysis of charge density difference (Fig. 4b) reveals the significant electronic interaction in W-O-Pdene. Then, the projected density of states (PDOS) of the Pd d-band is employed further to indicate the electronic interaction effects (Fig. 4c). The d-band center of W-O-Pdene (−1.768 eV) exhibits a downshift relative to that of Pdene (−1.465 eV), indicating that the electronic interaction of W-O-Pd can optimize the electronic structure of W-O-Pdene nanozymes and accelerate the desorption process of intermediates. Furthermore, Fig. 4d displays the schematic representation of the fundamental reaction step and energy change diagram of H_2O_2 activation on nanozymes. H_2O_2 is first absorbed on the W-O-Pd active sites. Then H_2O_2 is cleaved into two absorbed hydroxyl groups (OH*). Next, the two absorbed OH* are protonated to constitute H_2O* and desorb subsequently. W-O-Pdene nanozymes have a better capacity for capturing H_2O_2 because the adsorption energy of W-O-Pdene (−1.53 eV) is lower than that of Pdene (−1.03 eV). The step of desorption of the H_2O can be regarded as the rate-determining step (RDS). The RDS energy barrier of W-O-Pdene (0.82 eV) is lower than that of Pdene (1.19 eV), explaining the superiority of the POD-like activity of W-O-Pdene nanozymes. This result is consistent with the PDOS analysis. Besides, the weakened H_2O* binding on W-O-Pdene can be further evidenced by crystal orbital Hamilton population (COHP) analysis (Fig. 4e); pCOHP analysis reveals that the -ICOHP value at the Fermi level is lower for W-O-Pdene (2.434 eV) than that of Pdene (2.916 eV), which means that the H_2O* is easier to desorb on W-O-Pdene. Accordingly, W-O-Pdene nanozymes have high activity and specificity for the catalysis of H_2O_2, which is due to the synergistic effect of Pd sites and axial W atoms in the artificial 3D catalytic centers. On the one hand, the axial W atoms play an electronic role in the regulation of the Pd sites, resulting in a better desorption to enhance POD. On the other hand, the axial W atoms play an important role in binding for catalysis of H_2O_2, superior spatial configuration improving the specificity (Fig. S14†).

As the specific marker for prostate cancer, PSA has been widely used for the early diagnosis of prostate cancer during routine check-ups.[39–42] To investigate the potential application of W-O-Pdene for immunoassays, a colorimetric nanozyme-

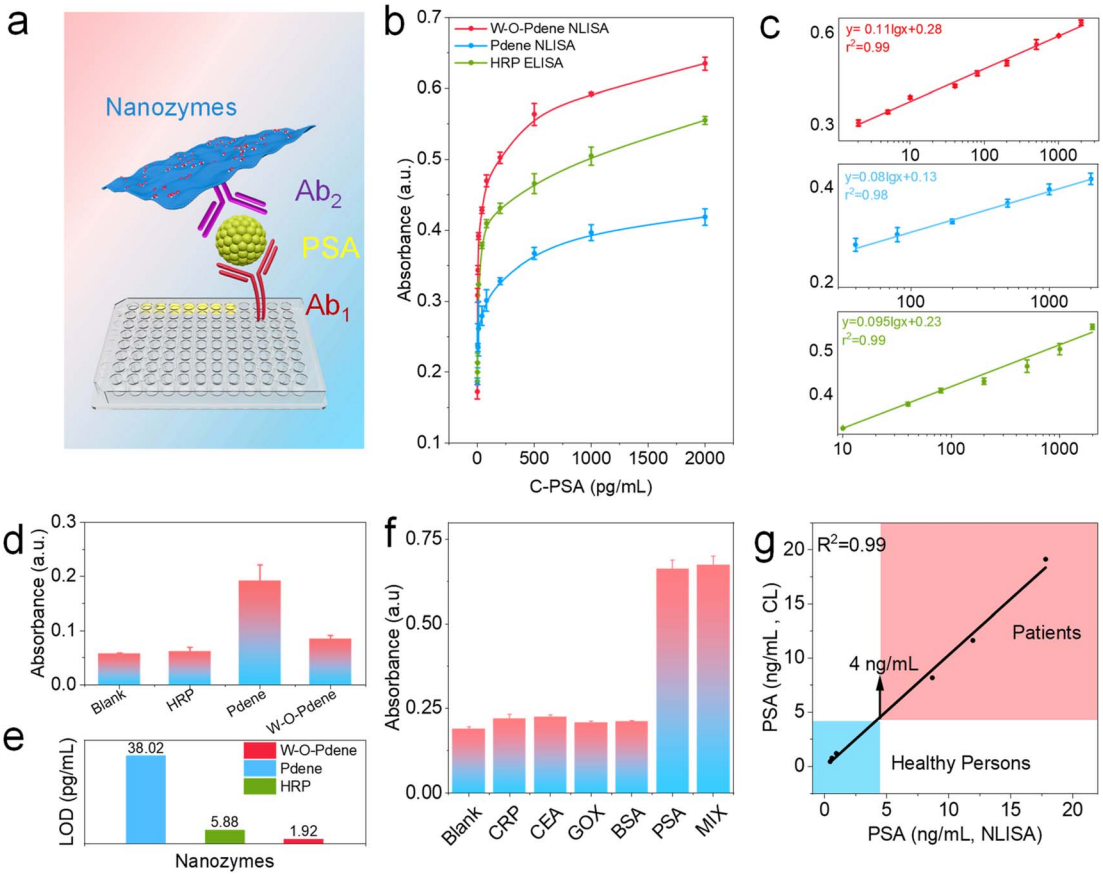

Fig. 5 (a) Schematic illustration of the colorimetric immunoassay of PSA. (b) Calibration curves of proposed W-O-Pdene-involved immunoassay and HRP-involved immunoassay. Linear ranges of the detection results from NLISA (C). (d) The background signals are caused by OXD-like activity. (e) LOD of different nanozyme-involved immunoassays. (f) Selectivity of W-O-Pdene-involved immunoassay. (g) The correlation curve of the NLISA method and the CL method of the real sample detection of PSA.

Open Access Article. Published on 26 August 2024. Downloaded on 2/8/2026 1:38:20 PM. This article is licensed under a Creative Commons Attribution-NonCommercial 3.0 Unported Licence.

linked immunosorbent assay (NLISA) of PSA was performed.[43–46] As displayed in Fig. 5a, NLISA is implemented through the typical sandwich immunoassay; anti-PSA coating monoclonal antibody (Ab_1) can capture the target PSA, subsequently, PSA is captured by anti-PSA labeling monoclonal antibody (Ab_2) to form the sandwich immunocomplexes. As displayed in Fig. 5b and c, with the increase of PSA concentration, the associated absorbance signals are consequently increased, demonstrating the feasibility of NILISA for the detection of PSA. The interference of dissolved oxygen with the background signal was investigated. As displayed in Fig. 5d, HRP has low background signals because of the superior specificity. Compared with Pdene nanozymes, W-O-Pdene nanozymes can decrease the background signal of immunoassay. Fig. 5e displays the limit of detection (LOD) of NLISA and ELISA. Interestingly, the LOD of W-O-Pdene-involved NLISA is determined to be 1.92 pg mL^{-1}, and the LOD of HRP-involved ELISA and Pdene-involved NLISA is calculated to be 5.88 and 38.02 pg mL^{-1}, respectively. The enhancement in the detection sensitivity for W-O-Pdene NLISA can be ascribed to the high catalytic efficiency and specificity of the W-O-Pdene. Furthermore, the specificity of PSA detection is demonstrated by the negligible responses observed for other biomarkers such as C-reactive protein (CRP), carcinoembryonic antigen (CEA), glucose oxidase (GOX), and bovine serum albumin (BSA) at a concentration of 2 ng mL^{-1} (Fig. 5f). Due to the superior sensing performance of NLISA, it is hopeful to be used in clinical diagnosis. Therefore, to verify the practicability in clinical diagnosis, NLISA was employed to detect human serum samples. As displayed in Fig. 5g and Table S5,† NLISA gets a linear fit greater than 99% with the chemiluminescence (CL) method in the hospital, verifying the practicability of NLISA in practical applications.

Conclusions

Inspired by the natural HRP catalytic pocket, W-O-Pdene nanozymes with artificial 3D catalytic centers are prepared successfully and demonstrate specific H_2O_2 activation efficiency. The catalytic activity and selectivity of W-O-Pdene nanozymes are systematically investigated based on experimental and theoretical analysis. 3D asymmetric W-O-Pd atomic pairs can selectively regulate the O–O bonding in H_2O_2 and O_2, and thus achieve the selective H_2O_2 activation. Besides, the asymmetric W-O-Pd atomic pairs can regulate the d-band center to accelerate the desorption of H_2O, which improves the catalytic activity of W-O-Pdene nanozymes. As a typical application, a colorimetric immunoassay for PSA is established, demonstrating better sensitivity than an enzyme-linked immunosorbent assay. This work offers new insight into fabricating unique POD-like nanozymes with high activity and selectivity.

Data availability

The data supporting this article have been included as part of the ESI.†

Author contributions

Conceptualization: L. J.; formal analysis: C. C., D. Y., X. J., R. L., L. H., and X. L.; funding acquisition: X. L., L. J., and Y. Z.; methodology: C. C. and L. J.; writing – original draft: C. C.; writing – review & editing: L. J., Y. Z., C. Z., and X. L. All authors discussed the results and assisted during manuscript preparation.

Conflicts of interest

There are no conflicts to declare.

Acknowledgements

The authors gratefully acknowledge the financial support of the National Natural Science Foundation of China (22174110, 22127803, and 22304096), the project ZR2023QB006 supported by Shandong Provincial Natural Science Foundation, supported by the China Postdoctoral Science Foundation under Grant Number 2023M741853, the Qingdao Postdoctoral Science Foundation (QDBSH20230202031), and the Plan for Youth Innovation Team of Colleges in Shandong Province.

Notes and references

1 H. Wei and E. Wang, *Chem. Soc. Rev.*, 2013, **42**, 6060–6093.
2 H. Fan, J. Zheng, J. Xie, J. Liu, X. Gao, X. Yan, K. Fan and L. Gao, *Adv. Mater.*, 2024, **36**, e2300387.
3 L. Zhang, H. Wang and X. Qu, *Adv. Mater.*, 2024, **36**, e2211147.
4 C. Peng, R. Pang, J. Li and E. Wang, *Adv. Mater.*, 2024, **36**, e2211724.
5 A. Zhang, A. Gao, C. Zhou, C. Xue, Q. Zhang, J. M. Fuente and D. Cui, *Adv. Mater.*, 2023, **35**, e2303722.
6 S. Zhang, Y. Li, S. Sun, L. Liu, X. Mu, S. Liu, M. Jiao, X. Chen, K. Chen, H. Ma, T. Li, X. Liu, H. Wang, J. Zhang, J. Yang and X. D. Zhang, *Nat. Commun.*, 2022, **13**, 4744.
7 Y. Wang and Y. Xianyu, *Small Methods*, 2022, **6**, e2101576.
8 D. Jiang, D. Ni, Z. T. Rosenkrans, P. Huang, X. Yan and W. Cai, *Chem. Soc. Rev.*, 2019, **48**, 3683–3704.
9 M. Liang and X. Yan, *Acc. Chem. Res.*, 2019, **52**, 2190–2200.
10 M. Zandieh and J. Liu, *Adv. Mater.*, 2024, **36**, e2211041.
11 C. Shang, Q. Wang, H. Tan, S. Lu, S. Wang, Q. Zhang, L. Gu, J. Li, E. Wang and S. Guo, *JACS Au*, 2022, **2**, 2453–2459.
12 L. Jiao, H. Yan, Y. Wu, W. Gu, C. Zhu, D. Du and Y. Lin, *Angew. Chem., Int. Ed.*, 2020, **59**, 2565–2576.
13 Y. Xu, Z. Zhou, N. Deng, K. Fu, C. Zhu, Q. Hong, Y. Shen, S. Liu and Y. Zhang, *Sci. China: Chem.*, 2023, **66**, 1318–1335.
14 Z. Zhang, X. Zhang, B. Liu and J. Liu, *J. Am. Chem. Soc.*, 2017, **139**, 5412–5419.
15 X. Chen, L. Zhao, K. Wu, H. Yang, Q. Zhou, Y. Xu, Y. Zheng, Y. Shen, S. Liu and Y. Zhang, *Chem. Sci.*, 2021, **12**, 8865–8871.
16 Z. Wang, R. Zhang, X. Yan and K. Fan, *Mater. Today*, 2020, **41**, 81–119.

© 2024 The Author(s). Published by the Royal Society of Chemistry

Open Access Article. Published on 26 August 2024. Downloaded on 2/8/2026 1:38:20 PM. This article is licensed under a Creative Commons Attribution-NonCommercial 3.0 Unported Licence.

17 Y. Chen, L. Jiao, H. Yan, W. Xu, Y. Wu, L. Zheng, W. Gu and C. Zhu, *Anal. Chem.*, 2021, **93**, 12353–12359.
18 Y. Wang, G. Jia, X. Cui, X. Zhao, Q. Zhang, L. Gu, L. Zheng, L. H. Li, Q. Wu, D. J. Singh, D. Matsumura, T. Tsuji, Y.-T. Cui, J. Zhao and W. Zheng, *Chem*, 2021, **7**, 436–449.
19 J. Han, H. Gong, X. Ren and X. Yan, *Nano Today*, 2021, **41**, 101295.
20 Y. Xu, A. Huang, W. Yi, G. Chen, S. Huang and G. Ouyang, *Coord. Chem. Rev.*, 2024, **500**, 215517.
21 Y. Xu, Z. Mao, J. Zhang, J. Ji, Y. Zou, M. Dong, B. Fu, M. Hu, K. Zhang, Z. Chen, S. Chen, H. Yin, P. Liu and H. Zhao, *Angew. Chem., Int. Ed.*, 2024, **63**, e202316029.
22 A. P. Green, T. Hayashi, P. R. E. Mittl and D. Hilvert, *J. Am. Chem. Soc.*, 2016, **138**, 11344–11352.
23 R. Geng, R. Chang, Q. Zou, G. Shen, T. Jiao and X. Yan, *Small*, 2021, **17**, e2008114.
24 L. Xie, X.-P. Zhang, B. Zhao, P. Li, J. Qi, X. Guo, B. Wang, H. Lei, W. Zhang, U.-P. Apfel and R. Cao, *Angew. Chem., Int. Ed.*, 2021, **60**, 7576–7581.
25 G. Li, H. Liu, T. Hu, F. Pu, J. Ren and X. Qu, *J. Am. Chem. Soc.*, 2023, **145**, 16835–16842.
26 P. Campomanes, U. Rothlisberger, M. Alfonso-Prieto and C. Rovira, *J. Am. Chem. Soc.*, 2015, **137**, 11170–11178.
27 W. Zhang, J. J. Dynes, Y. Hu, P. Jiang and S. Ma, *Nat. Commun.*, 2019, **10**, 1913.
28 Z. Lian, Y. Lu, S. Zhao, Z. Li and Q. Liu, *Adv. Sci.*, 2023, **10**, 2205975.
29 Z. Li, S. Ji, C. Xu, L. Leng, H. Liu, J. H. Horton, L. Du, J. Gao, C. He, X. Qi, Q. Xu and J. Zhu, *Adv. Mater.*, 2023, **35**, 2209644.
30 X. Li, G. Hai, J. Liu, F. Zhao, Z. Peng, H. Liu, M. K. H. Leung and H. Wang, *Appl. Catal., B*, 2022, **314**, 121531.
31 Q. Wang, K. Chen, H. Jiang, C. Chen, C. Xiong, M. Chen, J. Xu, X. Gao, S. Xu, H. Zhou and Y. Wu, *Nat. Commun.*, 2023, **14**, 5338.
32 B. Jiang, D. Duan, L. Gao, M. Zhou, K. Fan, Y. Tang, J. Xi, Y. Bi, Z. Tong, G. F. Gao, N. Xie, A. Tang, G. Nie, M. Liang and X. Yan, *Nat. Protoc.*, 2018, **13**, 1506–1520.
33 T. Chen, Y. Zhang and W. Xu, *J. Am. Chem. Soc.*, 2016, **138**, 12414–12421.
34 Z. D. Hood, H. Wang, A. Samuthira Pandian, J. K. Keum and C. Liang, *J. Am. Chem. Soc.*, 2016, **138**, 1768–1771.
35 S. E. Henkelis, M. Mazur, C. M. Rice, P. S. Wheatley, S. E. Ashbrook and R. E. Morris, *J. Am. Chem. Soc.*, 2019, **141**, 4453–4459.
36 S. Mondal, D. Bagchi, M. Riyaz, S. Sarkar, A. K. Singh, C. P. Vinod and S. C. Peter, *J. Am. Chem. Soc.*, 2022, **144**, 11859–11869.
37 Y. Wu, J. Wen, W. Xu, J. Huang, L. Jiao, Y. Tang, Y. Chen, H. Yan, S. Cao, L. Zheng, W. Gu, L. Hu, L. Zhang and C. Zhu, *Small*, 2021, **17**, e2101907.
38 Y. Tang, Y. Chen, Y. Wu, W. Xu, Z. Luo, H. R. Ye, W. Gu, W. Song, S. Guo and C. Zhu, *Nano Lett.*, 2023, **23**, 267–275.
39 Z. Xi, K. Wei, Q. Wang, M. J. Kim, S. Sun, V. Fung and X. Xia, *J. Am. Chem. Soc.*, 2021, **143**, 2660–2664.
40 S. Xie, X. Fei, J. Wang, Y.-C. Zhu, J. Liu, X. Du, X. Liu, L. Dong, Y. Zhu, J. Pan, B. Dong, J. Sha, Y. Luo, W. Sun and W. Xue, *Adv. Sci.*, 2023, **10**, 2206494.
41 L. Kachuri, T. J. Hoffmann, Y. Jiang, S. I. Berndt, J. P. Shelley, K. R. Schaffer, M. J. Machiela, N. D. Freedman, W. Y. Huang, S. A. Li, R. Easterlin, P. J. Goodman, C. Till, I. Thompson, H. Lilja, S. K. Van Den Eeden, S. J. Chanock, C. A. Haiman, D. V. Conti, R. J. Klein, J. D. Mosley, R. E. Graff and J. S. Witte, *Nat. Med.*, 2023, **29**, 1412–1423.
42 E. Shenderov, A. M. De Marzo, T. L. Lotan, H. Wang, S. Chan, S. J. Lim, H. Ji, M. E. Allaf, C. Chapman, P. A. Moore, F. Chen, K. Sorg, A. M. White, S. E. Church, B. Hudson, P. A. Fields, S. Hu, S. R. Denmeade, K. J. Pienta, C. P. Pavlovich, A. E. Ross, C. G. Drake, D. M. Pardoll and E. S. Antonarakis, *Nat. Med.*, 2023, **29**, 888–897.
43 M. Broto, M. M. Kaminski, C. Adrianus, N. Kim, R. Greensmith, S. Dissanayake-Perera, A. J. Schubert, X. Tan, H. Kim, A. S. Dighe, J. J. Collins and M. M. Stevens, *Nat. Nanotechnol.*, 2022, **17**, 1120–1126.
44 R. Li, H. Fan, H. Zhou, Y. Chen, Q. Yu, W. Hu, G. L. Liu and L. Huang, *Adv. Sci.*, 2023, **10**, 2301658.
45 Z. Farka, V. Čunderlová, V. Horáčková, M. Pastucha, Z. Mikušová, A. Hlaváček and P. Skládal, *Anal. Chem.*, 2018, **90**, 2348–2354.
46 N. Ye, S. Huang, H. Yang, T. Wu, L. Tong, F. Zhu, G. Chen and G. Ouyang, *Anal. Chem.*, 2021, **93**, 13981–13989.

© 2024 The Author(s). Published by the Royal Society of Chemistry